Licheng Cao, Lei Shao, Douwe J.J. van Hinsbergen, Tao Jiang, Di Xu, and Yuchi Cui, 2022, Provenance and evolution of East Asian large rivers recorded in the East and South China Seas: A review: GSA Bulletin, https://doi.org/10.1130/B36559.1.

Supplemental Material

Text. Description of the Studied Large River Basins.

Figures S1–S11.

Tables S1–S4.

Supplemental References.

Text. Description of the Studied Large River Basins.

Asia's largest river, the Yangtze River, is divided into three segments (Fig. 3). The headwater Jinsha River originates from the Qiangtang terrane with valleys deeply incising along the thrust contact between the Qiangtang and Songpan–Garze terranes where outcropping rocks are composed of Triassic turbidites and Triassic–Cenozoic granitic intrusions. Entering the Yangtze Craton, the mainstream is joined by several tributaries in the Sichuan Basin that is filled with Triassic–Cretaceous clastic rocks. After passing through the Three Gorges, the slope rapidly decreases and the middle reaches meander across the flat lowlands overlying the Jianghan Basin that is confined by the Qinling–Dabie Orogen to the north and the Jiangnan Orogen to the south. Farther eastward, the lower Yangtze River drains into the Subei Basin and the East China Sea.

The mainstream of the Pearl River, Xi River, originates from the southeastern plateau margin and confluences with two small tributaries (Bei and Dong Rivers) at the estuary, emptying into the northern South China Sea (Fig. 3). The upper Xi River mainly drains the Upper Paleozoic carbonates and Triassic turbidites of the Nanpanjiang Basin. The lower Xi River is joined by tributaries from the Neoproterozoic Jiangnan Orogen and flows through the Paleozoic strata and Yunkai Massif. To the east, the Bei and Dong Rivers drain Jurassic–Cretaceous intrusions of the East Cathaysia.

The Red River catchment is largely confined to the narrow, southeast-striking Ailao Shan-Red River fault zone (Fig. 3). Surrounding terranes, including Yangtze Craton and West Cathaysia to the northeast and Indochina to the south, render a complex range of outcropping rocks within the catchment. In general, the upstream region is dominated by the Paleozoic and Mesozoic sedimentary and metamorphic rocks, whereas the fault zone is characterized by several elongated high-grade metamorphic massifs and calc-alkaline to alkaline magmatic rocks. The mainstream confluences with two tributaries (Lo and Da Rivers) in the Hanoi Basin before discharging into the northwesternmost South China Sea.

Figures S1–S11.

Figure S1. Detrital zircon U-Pb age distributions of modern river sediments from East Asia, shown as a three-dimensional nonmetric multidimensional scaling (MDS) plot. Large and small rivers from different areas are color-coded. The orientation of the three-dimensional MDS plot is shown by projecting an individual sample (red circle) into three perpendicular planes. s—number of compiled samples. See Fig. 1B for sample localities and Table S1 for sampling information and references.

Figure S2. Detrital zircon U-Pb age distributions of modern river sediments from coastal South China (Chen et al., 2019; Li et al., 2021; Xu et al., 2007, 2014a, 2014a; Zhang et al., 2017a), shown as (A) a nonmetric multidimensional scaling (MDS) plot and (B–E) plots of kernel density estimation (KDE) spectra. In the MDS plot, solid and dashed lines mark the closest and the second closest neighbors, respectively. In the KDE plot, samples are grouped as a function of relative similarities of age signatures revealed by the MDS statistics. s—number of compiled samples, n-number of concordant analyses. See Fig. 1B for sample localities and Table S1 for sampling information and references.

Figure S3. Detrital K-feldspar Pb isotopic compositions of Upper Oligocene–Neogene strata from the northern Yinggehai Basin (Wang et al., 2019a; Zhang et al., 2021). Error bars are not shown for brevity. See Fig. 1B for sample localities and Table S2 for sampling information and references.

Figure S4. Schematic drainage reconstruction for Southeast China before (A) and after (B–D) the provenance shift of the Oligocene–Lower Miocene strata of West Taiwan (modified from Deng et al., 2017; Lan et al., 2016; Wang et al., 2018). Arrows stand for potential sediment dispersal routes. The provenance shift has been related to a drainage expansion of small rivers of coastal Southeast China (e.g., Min River; Lan et al., 2016) and an addition of a paleo–Yangtze River source either by long-distance sediment transport (Deng et al., 2017) or by sediment reworking of the East China Sea Shelf Basin (Wang et al., 2018).

Figure S5. Detrital zircon U-Pb age distributions of Upper Oligocene–Neogene strata from the margin of Hainan Island (Jiang et al., 2015; Lei et al., 2019; Lyu et al., 2021; Wang et al., 2015a, 2016, 2019b; Yan et al., 2011), shown as (A) a nonmetric multidimensional scaling (MDS) plot and (B-F) plots of kernel density estimation (KDE) spectra. In the MDS plot, solid and dashed lines mark the closest and the second closest neighbors, respectively. In the KDE plot, samples are grouped as a function of relative similarities of age signatures revealed by the MDS statistics. s—number of compiled samples, n—number of concordant analyses. See Fig. 1B for sample localities and Table S1 for sampling information and references.

Figure S6. Detrital zircon U-Pb age distributions of modern sediments from small rivers surrounding the northwestern South China Sea (Cao et al., 2015; Fyhn et al., 2019; Gong et al., 2021; He et al., 2020; Jonell et al., 2017; Usuki et al., 2013; Wang et al., 2015b, 2018a; Xu et al., 2014b), shown as (A) a nonmetric multidimensional scaling (MDS) plot and (B–D) plots of kernel density estimation (KDE) spectra. See Fig. S2 for legend description.

Figure S7. Detrital zircon U-Pb age distributions of Upper Cretaceous–Lower Paleogene strata from a range of inland basins along the eastern and southeastern margin of the Tibetan Plateau, using the compiled dataset (Chen et al., 2017b; Li et al., 2018; Wang et al., 2014b; Zhao et al., 2021) of Zhao (2021). Note that their raw dataset is slightly modified by excluding replicate samples (CX-25-2 and CX-31-2; Zhao et al., 2021) and implementing the strategy of this study in data treatment. Samples are grouped into stratigraphic intervals and compared by kernel density estimation (KDE) spectra, with grey bars marking different ages or magnitudes of key peaks within individual basins. s—number of compiled samples, n—number of concordant analyses.

Figure S8. Kernel density estimation (KDE) spectra of detrital zircon U-Pb ages from Paleogene strata of (A) the Jianchuan Basin (Clift et al., 2020; Feng et al., 2021; He et al., 2021; Wissink et al., 2016; Yan et al., 2012; Zheng et al., 2020) and (B) the Simao Basin (Chen et al., 2017b; Wissink et al., 2016). Samples from known formations are grouped. In the Jianchuan Basin, note the spectral difference between the Baoxiangsi–Jinsichang formations and the Shuanghe–Jianchuan formations. Samples Shi-12-02, Shi-12-01, Lij-12-01 have no age control and are interpreted to be equivalents of the Shuanghe–Jianchuan formations due to the presence of Paleogene zircons therein. In the Simao Basin, note that the age KDE spectrum of the Mengla Formation does show a multimodal pattern, contrasting with the original illustration of Chen et al. (2017b) that generally displays a unimodal pattern of age probability density spectrum peaking at ca. 220 Ma. Sample Jing-13-01 is tentatively assigned to the Mengla Formation because of their highly comparable age spectra.

Figure S9. Comparisons of detrital zircon age signatures among the modern sediments of the upper Yangtze River and Red River and the Paleogene formations of areas stretching from the Jianchuan Basin in the northwest to the Na Duong–Cao Bang Basins in the southeast, shown as (A) a nonmetric multidimensional scaling (MDS) plot and (B) plots of kernel density estimation (KDE) spectra. See Fig. S5 for legend description and Fig. 17 for the difference between the Na Duong–Cao Bang Basins (Clift et al., 2020) and the other datasets shown here.

Figure S10. Comparisons of detrital zircon age signatures of Upper Oligocene–Neogene strata among the Red River Basin (Clift et al., 2020; Hoang et al., 2009; Wissink et al., 2016), the Yinggehai Basin, and the Qiongdongnan Basin, shown as (A) a nonmetric multidimensional scaling (MDS) plot and (B–D) plots of kernel density estimation (KDE) spectra. See Fig. S5 for legend description and Fig. 14 for the dataset of the Yinggehai and Qiongdongnan Basins.

Figure S11. Cenozoic variation of sedimentation rate in (A) the East China Sea Shelf Basin (Clift, 2006), (B) the Pearl River Mouth Basin (Clift, 2006), and (C) the Yinggehai Basin (Hoang et al., 2010). Eo.–Eocene; Olig.–Oligocene; Mio.–Miocene; Plio.–Pliocene; L.–Lower; M.–Middle; U.–Upper.

Tables S1–S4.

Table S1. Compilation of detrital zircon U-Pb geochronology data from Cenozoic strata of key inland basins of East Asia and offshore basins of the China Seas as well as modern sediments in different rivers and offshore marine. Samples are listed in an order based on geographic localities in individual basins and rivers. For Cenozoic strata of the East and South China Seas, data are derived from the Xihu Sag of the East China Sea Shelf Basin (Wang et al., 2018c; Yang et al., 2006; Zhang et al., 2018), the Western Foothills and Hsuehshan Range of West Taiwan (Chen et al., 2017a; Lan et al., 2016; Yan et al., 2018), the northern sags of the Pearl River Mouth Basin (Cao et al., 2018; Fu et al., 2021; He et al., 2020; Shao et al., 2016, 2018; Wang et al., 2018b, 2017; Zhao, 2015), the western and central Qiongdongnan Basin (Lei et al., 2019; Lyu et al., 2021; Shao et al., 2016, 2018; Yan et al., 2011), as well as the Yinggehai Basin (Cao et al., 2015; Jiang et al., 2015; Wang et al., 2014a, 2015a, 2016, 2018a, 2019b, 2020b; Xie et al., 2016; Yan et al., 2011). For Cenozoic strata of inland basins, data are derived from the Jianghan Basin (Sun et al., 2018; Wang et al., 2014c; Yang et al., 2019), Nanjing area of the Subei Basin (Zheng et al., 2013), the Jianchuan Basin (Clift et al., 2020; Feng et al., 2021; He et al., 2021; Wissink et al., 2016; Yan et al., 2012; Zheng et al., 2020), the Simao Basin (Chen et al., 2017b; Wissink et al., 2016), the Red River Basin (Clift et al., 2020; Hoang et al., 2009; Wissink et al., 2016), and the Na Duong–Cao Bang Basins (Clift et al., 2020). For river sediments, data are derived from the Yangtze River (He et al., 2013, 2014; Hoang et al., 2009; Huang et al., 2020; Kong et al., 2009, 2011; Wang et al., 2020a; Yang et al., 2012), Southeast South China (Chen et al., 2019; Li et al., 2021; Xu et al., 2007, 2014a, 2014a; Zhang et al., 2017a), West Taiwan (Chen et al., 2019; Deng et al., 2017), the Pearl River (He et al., 2020; Liu et al., 2017; Zhao et al., 2015), Southwest South China (He et al., 2020), Hainan Island (Cao et al., 2015; Gong et al., 2021; Wang et al., 2015b; Xu et al., 2014b), the Red River (Clift et al., 2006a; Fyhn et al., 2019; Hoang et al., 2009; Wang et al., 2018a; Wissink et al., 2016), and Central Vietnam (Fyhn et al., 2019; Jonell et al., 2017; Usuki et al., 2013; Wang et al., 2018a). For marine sediments, data are derived from the East China Sea (Huang et al., 2020) and the northern South China Sea (Huang et al., 2020; Xu et al., 2016; Zhong et al., 2017). No extra common Pb correction is applied for the raw data. $^{206}Pb/^{238}U$ age is adopted for grains younger than 1000 Ma with discordance test calculated by [1-($^{206}Pb/^{238}U$ age / $^{207}Pb/^{206}Pb$ age)]*100, and $^{207}Pb/^{206}Pb$ age for those older than 1000 Ma with discordance test calculated by [1-($^{206}Pb/^{238}U$ age / $^{207}Pb/^{235}U$ age)]*100.

Table S2. Compilation of detrital K-feldspar Pb isotope data of modern sediments from the upper Yangtze River (Clift et al., 2008; Zhang et al., 2014, 2017b, 2020) and Red River (Bodet and Schärer, 2001; Clift et al., 2008), and Cenozoic strata from the Hanoi Basin (Clift et al., 2008) and northern Yinggehai Basin (Wang et al., 2019a; Zhang et al., 2021).

Table S3. Compilation of whole-Nd isotope data of Cenozoic strata from West Taiwan (Lan et al., 2014), the southern Pearl River Mouth Basin (Shao et al., 2015; Yan et al., 2018), and the adjacent continental-ocean transition zone (Li et al., 2003), the joint area of the Yinggehai–Qiongdongnan Basins (Yan et al., 2007), as well as the Hanoi Basin (Clift et al., 2006b).

Table S4. A summary of references for thermochronometric and paleoaltimetric results obtained from the eastern and southeastern margin of the Tibetan Plateau.

Supplemental References.

Bodet, F., and Schärer, U., 2001, Pb isotope systematics and time-integrated Th/U of SE-Asian continental crust recorded by single K-feldspar grains in large rivers: Chemical Geology, v. 177, p. 265–285, https://doi.org/10.1016/s0009-2541(00)00413-7.

Cao, L., Jiang, T., Wang, Z., Zhang, Y., and Sun, H., 2015, Provenance of Upper Miocene sediments in the Yinggehai and Qiongdongnan basins, northwestern South China Sea: Evidence from REE, heavy minerals and zircon U–Pb ages: Marine Geology, v. 361, p. 136–146, https://doi.org/10.1016/j.margeo.2015.01.007.

Cao, L., Shao, L., Qiao, P., Zhao, Z., and van Hinsbergen, D.J.J., 2018, Early Miocene birth of modern Pearl River recorded low-relief, high-elevation surface formation of SE Tibetan Plateau: Earth and Planetary Science Letters, v. 496, p. 120–131, https://doi.org/10.1016/j.epsl.2018.05.039.

Chen, C.-H., Lee, C.-Y., Lin, J.-W., and Chu, M.-F., 2019, Provenance of sediments in western Foothills and Hsuehshan Range (Taiwan): A new view based on the EMP monazite versus LA-ICPMS zircon geochronology of detrital grains: Earth-Science Reviews, v. 190, p. 224–246, https://doi.org/10.1016/j.earscirev.2018.12.015.

Chen, W.-S., Chung, S.-L., Chou, H.-Y., Zul, Z., Shao, W.-Y., and Lee, Y.-H., 2017a, A reinterpretation of the metamorphic Yuli belt: Evidence for a middle-late Miocene accretionary prism in eastern Taiwan: Tectonics, v. 36, p. 188–206, https://doi.org/10.1002/2016tc004383.

Chen, Y. et al., 2017b, Detrital zircon U–Pb geochronological and sedimentological study of the Simao Basin, Yunnan: Implications for the Early Cenozoic evolution of the Red River: Earth and Planetary Science Letters, v. 476, p. 22–33, https://doi.org/10.1016/j.epsl.2017.07.025.

Clift, P.D., 2006, Controls on the erosion of Cenozoic Asia and the flux of clastic sediment to the ocean: Earth and Planetary Science Letters, v. 241, p. 571–580, https://doi.org/10.1016/j.epsl.2005.11.028.

Clift, P.D., Carter, A., Campbell, I.H., Pringle, M.S., Van Lap, N., Allen, C.M., Hodges, K.V., and Tan, M.T., 2006a, Thermochronology of mineral grains in the Red and Mekong Rivers, Vietnam: provenance and exhumation implications for Southeast Asia: Geochemistry, Geophysics, Geosystems, v. 7, Q10005, https://doi.org/10.1029/2006gc001336.

Clift, P.D., Blusztajn, J., and Nguyen, A.D., 2006b, Large-scale drainage capture and surface uplift in eastern Tibet-SW China before 24 Ma inferred from sediments of the Hanoi Basin, Vietnam: Geophysical Research Letters, v. 33, L19403, https://doi.org/10.1029/2006gl027772.

Clift, P.D., van Hoang, L., Hinton, R., Ellam, R.M., Hannigan, R., Tan, M.T., Blusztajn, J., and Duc, N.A., 2008, Evolving east Asian river systems reconstructed by trace element and Pb and Nd isotope variations in modern and ancient Red River-Song Hong sediments: Geochemistry, Geophysics, Geosystems, v. 9, Q04039, https://doi.org/10.1029/2007gc001867.

Clift, P.D., Carter, A., Wysocka, A., Hoang, L.V., Zheng, H.B., and Neubeck, N., 2020, A Late Eocene-Oligocene through-flowing river Between the upper Yangtze and South China Sea: Geochemistry, Geophysics, Geosystems, v. 21, e2020GC009046, https://doi.org/10.1029/2020GC009046.

Deng, K., Yang, S., Li, C., Su, N., Bi, L., Chang, Y.-P., and Chang, S.-C., 2017, Detrital zircon geochronology of river sands from Taiwan: Implications for sedimentary provenance of Taiwan and its source link with the east China mainland: Earth-Science Reviews, v. 164, p. 31–47, https://doi.org/10.1016/j.earscirev.2016.10.015.

Feng, Y., Song, C., He, P., Meng, Q., Wang, Q., Wang, X., and Chen, W., 2021, Detrital zircon U-Pb geochronology of the Jianchuan Basin, southeastern Tibetan Plateau, and its implications for tectonic and paleodrainage evolution: Terra Nova, v. 33, p. 560–572, https://doi.org/10.1111/ter.12548.

Fu, C., Li, S., Li, S., and Xu, J., 2021, Spatial and temporal variability of sediment infilling and episodic rifting in the North Pearl River Mouth Basin, South China Sea: Journal of Asian Earth Sciences, v. 211, 104702, https://doi.org/10.1016/j.jseaes.2021.104702.

Fyhn, M.B.W. et al., 2019, Detrital zircon ages and heavy mineral composition along the Gulf of Tonkin - Implication for sand provenance in the Yinggehai-Song Hong and Qiongdongnan basins: Marine and Petroleum Geology, v. 101, p. 162–179, https://doi.org/10.1016/j.marpetgeo.2018.11.051.

Gong, Y., Pease, V., Wang, H., Gan, H., Liu, E., Ma, Q., Zhao, S., and He, J., 2021, Insights into evolution of a rift basin: Provenance of the middle Eocene-lower Oligocene strata of the Beibuwan Basin, South China Sea from detrital zircon: Sedimentary Geology, v. 419, 105908, https://doi.org/10.1016/j.sedgeo.2021.105908.

He, J., Garzanti, E., Cao, L., and Wang, H., 2020, The zircon story of the Pearl River (China) from Cretaceous to present: Earth-Science Reviews, v. 201, 103078, https://doi.org/10.1016/j.earscirev.2019.103078.

He, M., Zheng, H., and Clift, P.D., 2013, Zircon U–Pb geochronology and Hf isotope data from the Yangtze River sands: Implications for major magmatic events and crustal evolution in Central China: Chemical Geology, v. 360–361, p. 186–203, https://doi.org/10.1016/j.chemgeo.2013.10.020.

He, M., Zheng, H., Bookhagen, B., and Clift, P.D., 2014, Controls on erosion intensity in the Yangtze River basin tracked by U–Pb detrital zircon dating: Earth-Science Reviews, v. 136, p. 121–140, https://doi.org/10.1016/j.earscirev.2014.05.014.

He, M., Zheng, H., Clift, P.D., Bian, Z., Yang, Q., Zhang, B., and Xia, L., 2021, Paleogene Sedimentary Records of the Paleo-Jinshajiang (Upper Yangtze) in the Jianchuan Basin, Yunnan, SW China: Geochemistry, Geophysics, Geosystems, v. 22, e2020GC009500, https://doi.org/10.1029/2020gc009500.

Hoang, L.V., Wu, F., Clift, P.D., Wysocka, A., and Swierczewska, A., 2009, Evaluating the evolution of the Red River system based on in situ U–Pb dating and Hf isotope analysis of zircons: Geochemistry, Geophysics, Geosystems, v. 10, Q11008, https://doi.org/10.1029/2009gc002819.

Hoang, L.V., Clift, P.D., Schwab, A.M., Huuse, M., Nguyen, D.A., and Sun, Z., 2010, Large-scale erosional response of SE Asia to monsoon evolution reconstructed from sedimentary records of the Song Hong-Yinggehai and Qiongdongnan basins, South China Sea, *in* Clift, P.D., Tada, R., and Zheng, H. eds., Monsoon Evolution and Tectonics-Climate Linkage in Asia, London, Geological Society Publishing House, Geological Society, London, Special Publications, v. 342, p. 219–244, https://doi.org/10.1144/sp342.13.

Huang, X., Song, J., Yue, W., Wang, Z., Mei, X., Li, Y., Li, F., Lian, E., and Yang, S., 2020, Detrital zircon U-Pb ages in the East China Seas: Implications for provenance analysis and sediment budgeting: Minerals, v. 10, 398, https://doi.org/10.3390/min10050398.

Jiang, T., Cao, L., Xie, X., Wang, Z., Li, X., Zhang, Y., Zhang, D., and Sun, H., 2015, Insights from heavy minerals and zircon U–Pb ages into the middle Miocene–Pliocene provenance evolution of the Yinggehai Basin, northwestern South China Sea: Sedimentary Geology, v. 327, p. 32–42, https://doi.org/10.1016/j.sedgeo.2015.07.011.

Jonell, T.N., Clift, P.D., Hoang, L.V., Hoang, T., Carter, A., Wittmann, H., Böning, P., Pahnke, K., and Rittenour, T., 2017, Controls on erosion patterns and sediment transport in a monsoonal, tectonically quiescent drainage, Song Gianh, central Vietnam: Basin Research, v. 29, p. 659–683, https://doi.org/10.1111/bre.12199.

Kong, P., Granger, D., Wu, F., Caffee, M., Wang, Y., Zhao, X., and Zheng, Y., 2009, Cosmogenic nuclide burial ages and provenance of the Xigeda paleo-lake: Implications for evolution of the Middle Yangtze River: Earth and Planetary Science Letters, v. 278, p. 131–141, https://doi.org/10.1016/j.epsl.2008.12.003.

Kong, P., Zheng, Y., and Fu, B., 2011, Cosmogenic nuclide burial ages and provenance of Late Cenozoic deposits in the Sichuan Basin: Implications for Early Quaternary glaciations in east Tibet: Quaternary Geochronology, v. 6, p. 304–312, https://doi.org/10.1016/j.quageo.2011.03.006.

Lan, Q., Yan, Y., Huang, C.-Y., Clift, P.D., Li, X., Chen, W., Zhang, X., and Yu, M., 2014, Tectonics, topography, and river system transition in East Tibet: Insights from the sedimentary record in Taiwan: Geochemistry, Geophysics, Geosystems, v. 15, p. 3658–3674, https://doi.org/10.1002/2014GC005310.

Lan, Q., Yan, Y., Huang, C.-Y., Santosh, M., Shan, Y.-H., Chen, W., Yu, M., and Qian, K., 2016, Topographic architecture and drainage reorganization in Southeast China: Zircon U-Pb chronology and Hf isotope evidence from Taiwan: Gondwana Research, v. 36, p. 376–389, https://doi.org/10.1016/j.gr.2015.07.008.

Lei, C., Clift, P.D., Ren, J., Ogg, J., and Tong, C., 2019, A rapid shift in the sediment routing system of Lower-Upper Oligocene strata in the Qiongdongnan Basin (Xisha Trough), Northwest South China Sea: Marine and Petroleum Geology, v. 104, p. 249–258, https://doi.org/10.1016/j.marpetgeo.2019.03.012.

Li, X.H., Wei, G.J., Shao, L., Liu, Y., Liang, X.R., Han, Z.M., Sun, M., and Wang, P.X., 2003, Geochemical and Nd isotopic variations in sediments of the South China Sea: a response to Cenozoic tectonism in SE Asia: Earth and Planetary Science Letters, v. 211, p. 207–220, https://doi.org/10.1016/S0012-821x(03)00229-2.

Li, Y., He, D., Li, D., Lu, R., Fan, C., Sun, Y., and Huang, H., 2018, Sedimentary provenance constraints on the Jurassic to Cretaceous paleogeography of Sichuan Basin, SW China: Gondwana Research, v. 60, p. 15–33, https://doi.org/10.1016/j.gr.2018.03.015.

Li, Y., Huang, X., Hiep, N.T., Lian, E., and Yang, S., 2021, Disentangle the sediment mixing from geochemical proxies and detrital zircon geochronology: Marine Geology, v. 440, 106572, https://doi.org/10.1016/j.margeo.2021.106572.

Liu, C., Clift, P.D., Carter, A., Böning, P., Hu, Z., Sun, Z., and Pahnke, K., 2017, Controls on modern erosion and the development of the Pearl River drainage in the late Paleogene: Marine Geology, v. 394, p. 52–68, https://doi.org/10.1016/j.margeo.2017.07.011.

Lyu, C., Li, C., Chen, G., Zhang, G., Ma, M., Zhang, Y., Sun, Z., and Zhou, Q., 2021, Zircon U–Pb age constraints on the provenance of Upper Oligocene to Upper Miocene sandstones in the western Qiongdongnan Basin, South China Sea: Marine and Petroleum Geology, v. 126, 104891, https://doi.org/10.1016/j.marpetgeo.2020.104891.

Shao, L., Qiao, P., Zhao, M., Li, Q., Wu, M., Pang, X., and Zhang, H., 2015, Depositional characteristics of the northern South China Sea in response to the evolution of the Pearl River, *in* Clift, P.D., Harff, J., Wu, J., and Qui, Y., eds., River-Dominated Shelf Sediments of East Asian Seas: Geological Society, London, Special Publications, v. 429, p. 31–44, https://doi.org/10.1144/SP429.2.

Shao, L., Cao, L., Pang, X., Jiang, T., Qiao, P., and Zhao, M., 2016, Detrital zircon provenance of the Paleogene syn-rift sediments in the northern South China Sea: Geochemistry, Geophysics, Geosystems, v. 17, p. 255–269, https://doi.org/10.1002/2015GC006113.

Shao, L., Cui, Y., Stattegger, K., Zhu, W., Qiao, P., and Zhao, Z., 2018, Drainage control of Eocene to Miocene sedimentary records in the southeastern margin of Eurasian Plate: Geological Society of America Bulletin, v. 131, p. 461–478, https://doi.org/10.1130/b32053.1.

Sun, X., Li, C., Kuiper, K.F., Wang, J., Tian, Y., Vermeesch, P., Zhang, Z., Zhao, J., and Wijbrans, J.R., 2018, Geochronology of detrital muscovite and zircon constrains the sediment provenance changes in the Yangtze River during the late Cenozoic: Basin Research, v. 30, p. 636–649, https://doi.org/10.1111/bre.12268.

Usuki, T., Lan, C.-Y., Wang, K.-L., and Chiu, H.-Y., 2013, Linking the Indochina block and Gondwana during the Early Paleozoic: Evidence from U–Pb ages and Hf isotopes of detrital zircons: Tectonophysics, v. 586, p. 145–159, https://doi.org/10.1016/j.tecto.2012.11.010.

Wang, A., Li, X., Luo, X., Santosh, M., Cui, Y., Li, Q., Lai, D., Wan, J., and Zhang, X., 2020a, Crustal growth as revealed by integrated U–Pb and Lu–Hf isotope analyses of detrital zircons from the Ganjiang River, southeastern China: Geological Magazine, v. 157, p. 666–676, https://doi.org/10.1017/s001675681900116x.

Wang, C. et al., 2014a, Provenance of Upper Miocene to Quaternary sediments in the Yinggehai-Song Hong Basin, South China Sea: evidence from detrital zircon U–Pb ages: Marine Geology, v. 355, p. 202–217, https://doi.org/10.1016/j.margeo.2014.06.004.

Wang, C., Liang, X., Xie, Y., Tong, C., Pei, J., Zhou, Y., Jiang, Y., Fu, J., and Wen, S., 2015a, Late Miocene provenance change on the eastern margin of the Yinggehai-Song Hong Basin, South China Sea: Evidence from U–Pb dating and Hf isotope analyses of detrital zircons: Marine and Petroleum Geology, v. 61, p. 123–139, https://doi.org/10/f64328.

Wang, C. et al., 2015b, Construction of age frequencies of provenances on the eastern side of the Yinggehai Basin: Studies of LA-ICP-MS U-Pb ages of detrital zircons from six modern rivers, western Hainan, China: Earth Science Frontiers, v. 22, p. 277- 289 [in Chinese with English abstract], https://doi.org/10.13745/j.esf.2015.04.028.

Wang, C. et al., 2016, Zircon U-Pb geochronology and heavy mineral composition constraints on the provenance of the middle Miocene deep-water reservoir sedimentary rocks in the Yinggehai-Song Hong Basin, South China Sea: Marine and Petroleum Geology, v. 77, p. 819–834, https://doi.org/10.1016/j.marpetgeo.2016.05.009.

Wang, C., Liang, X., Foster, D.A., Tong, C., Liu, P., Liang, X., and Zhang, L., 2018a, Linking source and sink: Detrital zircon provenance record of drainage systems in Vietnam and the Yinggehai–Song Hong Basin, South China Sea: Geological Society of America Bulletin, v. 131, p. 191–204, https://doi.org/10.1130/b32007.1.

Wang, C., Wen, S., Liang, X., Shi, H., and Liang, X., 2018b, Detrital zircon provenance record of the Oligocene Zhuhai Formation in the Pearl River Mouth Basin, northern South China Sea: Marine and Petroleum Geology, v. 98, p. 448–461, https://doi.org/10.1016/j.marpetgeo.2018.08.032.

Wang, C., Liang, X., Foster, D.A., Liang, X., Zhang, L., and Su, M., 2019a, Provenance and drainage evolution of the Red River revealed by Pb isotopic analysis of detrital K-feldspar: Geophysical Research Letters, v. 46, p. 6415–6424, https://doi.org/10.1029/2019gl083000.

Wang, C., Liang, X., Foster, D.A., Liang, X., Tong, C., and Liu, P., 2019b, Detrital zircon ages: A key to unraveling provenance variations in the eastern Yinggehai–Song Hong Basin, South China Sea: AAPG Bulletin, v. 103, p. 1525–1552, https://doi.org/10.1306/11211817270.

Wang, C., Zeng, L., Lei, Y., Su, M., and Liang, X., 2020b, Tracking the detrital zircon provenance of Early Miocene sediments in the continental shelf of the northwestern South China Sea: Minerals, v. 10, 752, https://doi.org/10.3390/min10090752.

Wang, L., Liu, C., Gao, X., and Zhang, H., 2014b, Provenance and paleogeography of the Late Cretaceous Mengyejing Formation, Simao Basin, southeastern Tibetan Plateau: Whole-rock geochemistry, U–Pb geochronology, and Hf isotopic constraints: Sedimentary Geology, v. 304, p. 44–58, https://doi.org/10.1016/j.sedgeo.2014.02.003.

Wang, P., Zheng, H., Chen, L., Chen, J., Xu, Y., Wei, X., and Yao, X., 2014c, Exhumation of the Huangling anticline in the Three Gorges region: Cenozoic sedimentary record from the western Jianghan Basin, China: Basin Research, v. 26, p. 505–522, https://doi.org/10.1111/bre.12047.

Wang, W., Ye, J., Bidgoli, T., Yang, X., Shi, H., and Shu, Y., 2017, Using detrital zircon geochronology to constrain Paleogene provenance and its relationship to rifting in the Zhu 1 Depression, Pearl River Mouth Basin, South China Sea: Geochemistry, Geophysics, Geosystems, v. 18, p. 3976–3999, https://doi.org/10.1002/2017gc007110.

Wang, W., Bidgoli, T., Yang, X., and Ye, J., 2018c, Source-to-sink links between East Asia and Taiwan from detrital zircon geochronology of the Oligocene Huagang Formation in the East China Sea Shelf Basin: Geochemistry, Geophysics, Geosystems, v. 19, p. 3673–3688, https://doi.org/10.1029/2018gc007576.

Wissink, G.K., Hoke, G.D., Garzione, C.N., and Liu-Zeng, J., 2016, Temporal and spatial patterns of sediment routing across the southeast margin of the Tibetan Plateau: Insights from detrital zircon: Tectonics, v. 35, p. 2538–2563, https://doi.org/10.1002/2016tc004252.

Xie, Y., Li, X., Fan, C., Tan, J., Liu, K., Lu, Y., Hu, W., Li, H., and Wu, J., 2016, The axial channel provenance system and natural gas accumulation of the Upper Miocene Huangliu Formation in Qiongdongnan Basin, South China Sea: Petroleum Exploration and Development, v. 43, p. 570–578, https://doi.org/10.1016/s1876-3804(16)30067-2.

Xu, X., O'Reilly, S.Y., Griffin, W.L., Wang, X., Pearson, N.J., and He, Z., 2007, The crust of Cathaysia: Age, assembly and reworking of two terranes: Precambrian Research, v. 158, p. 51–78, https://doi.org/10.1016/j.precamres.2007.04.010.

Xu, Y., Sun, Q., Yi, L., Yin, X., Wang, A., Li, Y., and Chen, J., 2014a, Detrital zircons U-Pb age and Hf isotope from the western side of the Taiwan Strait: Implications for sediment provenance and crustal evolution of the northeast Cathaysia Block: Terrestrial, Atmospheric and Oceanic Sciences, v. 25, p. 505–535, https://doi.org/10.3319/TAO.2014.02.18.01(TT).

Xu, Y., Sun, Q., Cai, G., Yin, X., and Chen, J., 2014b, The U–Pb ages and Hf isotopes of detrital zircons from Hainan Island, South China: implications for sediment provenance and the crustal evolution: Environmental Earth Sciences, v. 71, p. 1619–1628, https://doi.org/10.1007/s12665-013-2566-x.

Xu, Y., Wang, C.Y., and Zhao, T., 2016, Using detrital zircons from river sands to constrain major tectono-thermal events of the Cathaysia Block, SE China: Journal of Asian Earth Sciences, v. 124, p. 1–13, https://doi.org/10.1016/j.jseaes.2016.04.012.

Yan, Y., Xia, B., Lin, G., Carter, A., Hu, X.Q., Cui, X.J., Liu, B.M., Yan, P., and Song, Z.J., 2007, Geochemical and Nd isotope composition of detrital sediments on the north margin of the South China Sea: provenance and tectonic implications: Sedimentology, v. 54, p. 1–17, https://doi.org/10.1111/j.1365-3091.2006.00816.x.

Yan, Y., Carter, A., Palk, C., Brichau, S., and Hu, X.Q., 2011, Understanding sedimentation in the Song Hong-Yinggehai Basin, South China Sea: Geochemistry, Geophysics, Geosystems, v. 12, Q06014, https://doi.org/10.1029/2011gc003533.

Yan, Y., Carter, A., Huang, C.-Y., Chan, L.-S., Hu, X.-Q., and Lan, Q., 2012, Constraints on Cenozoic regional drainage evolution of SW China from the provenance of the Jianchuan Basin: Geochemistry, Geophysics, Geosystems, v. 13, Q03001, https://doi.org/10.1029/2011gc003803.

Yan, Y., Yao, D., Tian, Z.-X., Huang, C.-Y., Dilek, Y., Clift, P.D., and Li, Z.-A., 2018, Tectonic topography changes in Cenozoic East Asia: A landscape erosion-sediment archive in the South China Sea: Geochemistry, Geophysics, Geosystems, v. 19, p. 1731–1750, https://doi.org/10.1029/2017gc007356.

Yang, C., Shen, C., Zattin, M., Yu, W., Shi, S., and Mei, L., 2019, Provenances of Cenozoic sediments in the Jianghan Basin and implications for the formation of the Three Gorges: International Geology Review, v. 61, p. 1980–1999, https://doi.org/10.1080/00206814.2019.1576066.

Yang, S., Zhang, F., and Wang, Z., 2012, Grain size distribution and age population of detrital zircons from the Changjiang (Yangtze) River system, China: Chemical Geology, v. 296–297, p. 26–38, https://doi.org/10.1016/j.chemgeo.2011.12.016.

Yang, X., Li, A., Qin, Y., Wu, S., Wu, Z., and Zhang, J., 2006, U-Pb dating of zircons from Cenozoic sandstone: constrain on the geodynamic setting of East China Sea Shelf Basin: Marine Geology & Quaternary Geology, v. 26, p. 75–85.

Zhang, J. et al., 2018, Source to sink transport in the Oligocene Huagang Formation of the Xihu Depression, East China Sea Shelf Basin: Marine and Petroleum Geology, v. 98, p. 733–745, https://doi.org/10.1016/j.marpetgeo.2018.09.014.

Zhang, X.C., Huang, C.Y., Wang, Y.J., Clift, P.D., Yan, Y., Fu, X.W., and Chen, D.F., 2017a, Evolving Yangtze River reconstructed by detrital zircon U-Pb dating and petrographic analysis of Miocene marginal Sea sedimentary rocks of the Western Foothills and Hengchun Peninsula, Taiwan: Tectonics, v. 36, p. 634–651, https://doi.org/10.1002/2016tc004357.

Zhang, Z., Tyrrell, S., Li, C., Daly, J.S., Sun, X., and Li, Q., 2014, Pb isotope compositions of detrital K-feldspar grains in the upper-middle Yangtze River system: Implications for sediment provenance and drainage evolution: Geochemistry, Geophysics, Geosystems, v. 15, p. 2765–2779, https://doi.org/10.1002/2014gc005391.

Zhang, Z., Daly, J.S., Li, C., Tyrrell, S., Sun, X., and Yan, Y., 2017b, Sedimentary provenance constraints on drainage evolution models for SE Tibet: evidence from detrital K-feldspar: Geophysical Research Letters, v. 44, p. 4064–4073, https://doi.org/10.1002/2017gl073185.

Zhang, Z., Daly, J.S., Li, C., Tyrrell, S., Badenszki, E., Sun, X., Tian, Y., and Yan, Y., 2020, Southeastern Tibetan Plateau serves as the dominant sand contributor to the Yangtze River:

evidence from Pb isotopic compositions of detrital K-feldspar: Terra Nova, v. 33, p. 195–207, https://doi.org/10.1111/ter.12505.
Zhang, Z., Daly, J.S., Yan, Y., Lei, C., Badenszki, E., Sun, X., and Tian, Y., 2021, No connection between the Yangtze and Red rivers since the late Eocene: Marine and Petroleum Geology, v. 129, 105115, https://doi.org/10.1016/j.marpetgeo.2021.105115.
Zhao, M., 2015, The evolution of the Pearl River and its sedimentary record in the northern South China Sea: Shanghai, China, Tongji University, 124 p.
Zhao, M., Shao, L., and Qiao, P., 2015, Characteristics of detrital zircon U-Pb geochronology of the Pearl River sands and its implication on provenances: Journal of Tongji University (Natural Science), v. 43, p. 89–97 [in Chinese with English abstract], https://doi.org/10.11908/j.issn.0253-374x.2015.06.018.
Zhao, X. et al., 2021, Existence of a continental-scale river system in eastern Tibet during the late Cretaceous–early Palaeogene: Nature Communications, v. 12, 7231, https://doi.org/10.1038/s41467-021-27587-9.
Zheng, H., Clift, P.D., Wang, P., Tada, R., Jia, J., Hee, M., and Jourdanf, F., 2013, Pre-Miocene birth of the Yangtze River: Proceedings of the National Academy of Sciences of the United States of America, v. 110, p. 7556–7561, https://doi.org/10.1073/pnas.1216241110.
Zheng, H., Clift, P.D., He, M., Bian, Z., Liu, G., Liu, X., Xia, L., Yang, Q., and Jourdan, F., 2020, Formation of the First Bend in the late Eocene gave birth to the modern Yangtze River, China: Geology, v. 49, p. 35–39, https://doi.org/10.1130/g48149.1.
Zhong, L., Li, G., Yan, W., Xia, B., Feng, Y., Miao, L., and Zhao, J., 2017, Using zircon U–Pb ages to constrain the provenance and transport of heavy minerals within the northwestern shelf of the South China Sea: Journal of Asian Earth Sciences, v. 134, p. 176–190, https://doi.org/10.1016/j.jseaes.2016.11.019.

Figure S1

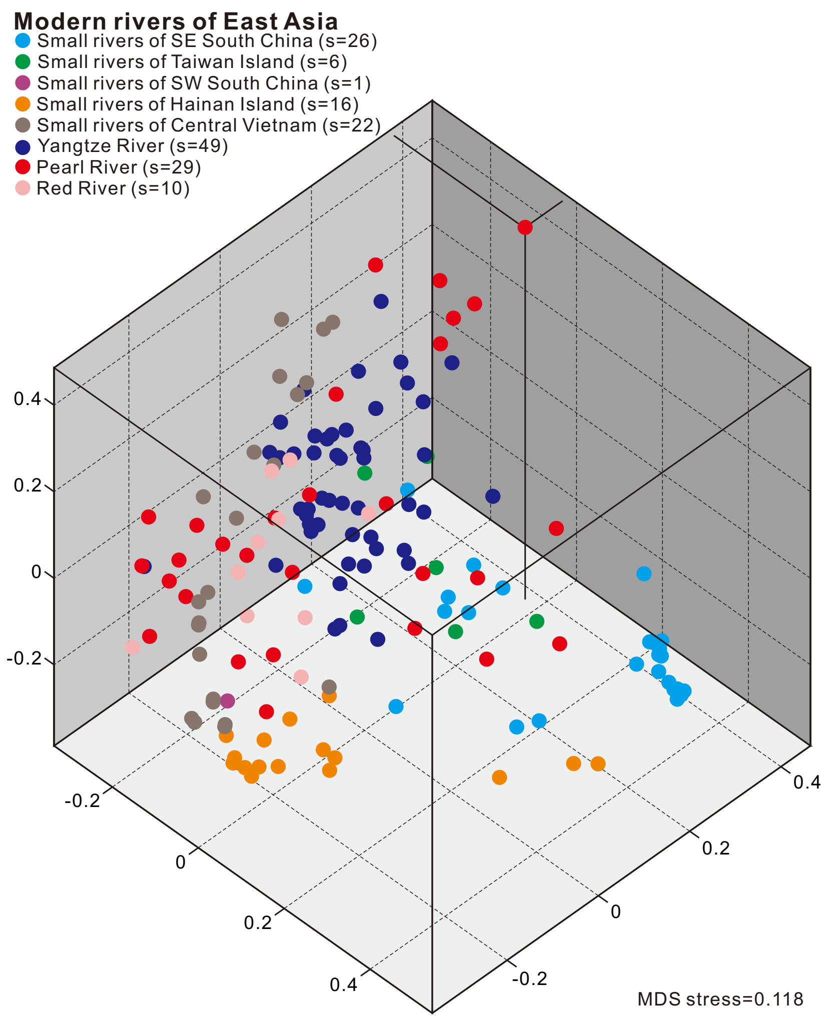

Modern rivers of East Asia
Small rivers of SE South China (s=26)
Small rivers of Taiwan Island (s=6)
Small rivers of SW South China (s=1)
Small rivers of Hainan Island (s=16)
Small rivers of Central Vietnam (s=22)
Yangtze River (s=49)
Pearl River (s=29)
Red River (s=10)
0.4
0.2
0
-0.2
-0.2
0
0.2
0.4
0.4
0.2
0
-0.2
MDS stress=0.118

Figure S2

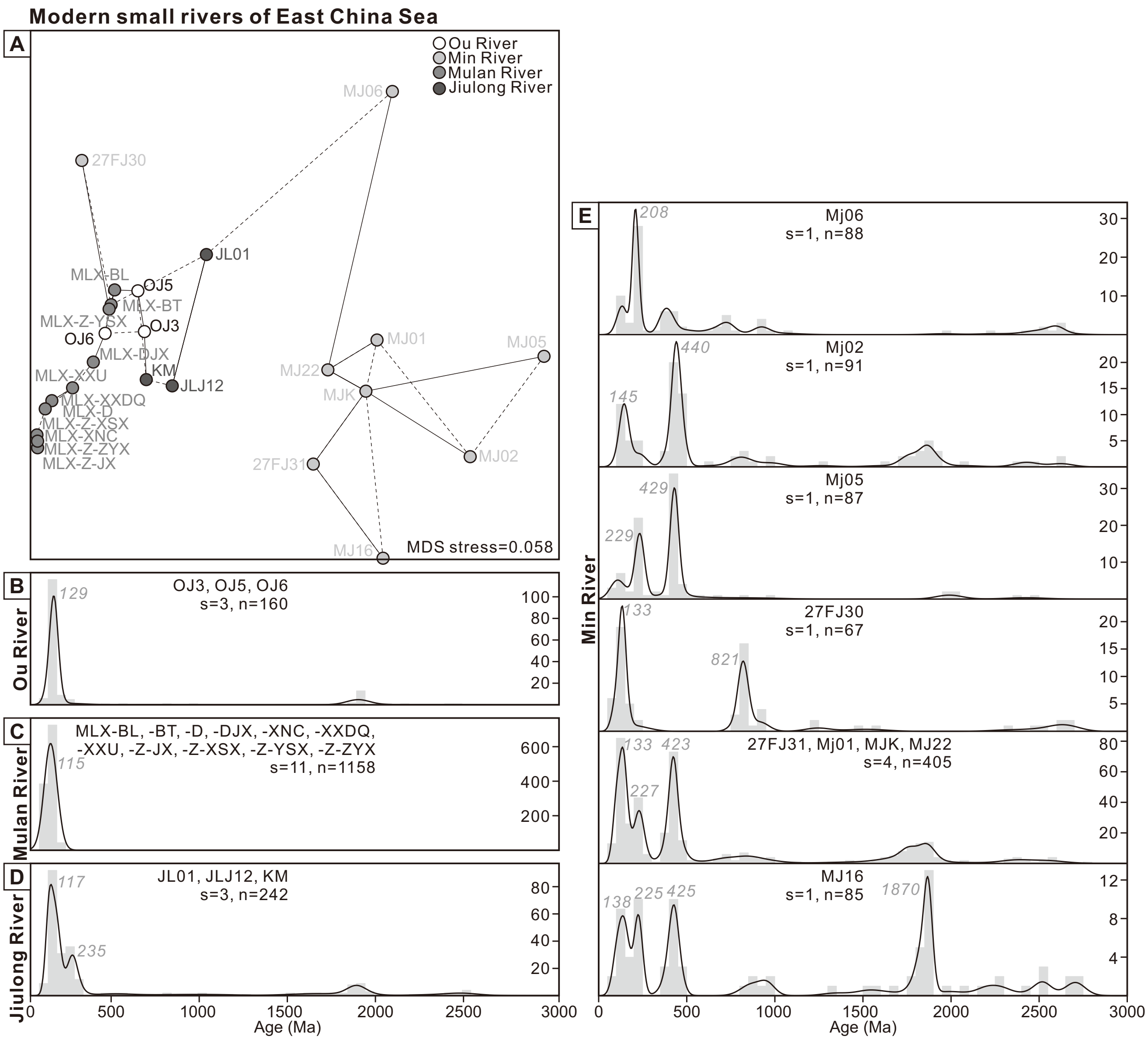
Modern small rivers of East China Sea
A
Ou River
Min River
Mulan River
Jiulong River
MJ06
27FJ30
JL01
MLX-BL
OJ5
MLX-BT
MLX-Z-YSX
OJ3
OJ6
MLX-DJX
MJ01
MJ05
MJ22
KM
JLJ12
MLX-XXU
MJK
MLX-XXDQ
MLX-D
MLX-Z-XSX
MLX-XNC
MLX-Z-ZYX
MLX-Z-JX
MJ02
27FJ31
MJ16
MDS stress=0.058
B
Ou River
129
OJ3, OJ5, OJ6
s=3, n=160
C
Mulan River
115
MLX-BL, -BT, -D, -DJX, -XNC, -XXDQ,
-XXU, -Z-JX, -Z-XSX, -Z-YSX, -Z-ZYX
s=11, n=1158
D
Jiulong River
117
235
JL01, JLJ12, KM
s=3, n=242
Age (Ma)
E
Min River
208
Mj06
s=1, n=88
145
440
Mj02
s=1, n=91
229
429
Mj05
s=1, n=87
133
821
27FJ30
s=1, n=67
133
227
423
27FJ31, Mj01, MJK, MJ22
s=4, n=405
138
225
425
1870
MJ16
s=1, n=85
Age (Ma)

Figure S3

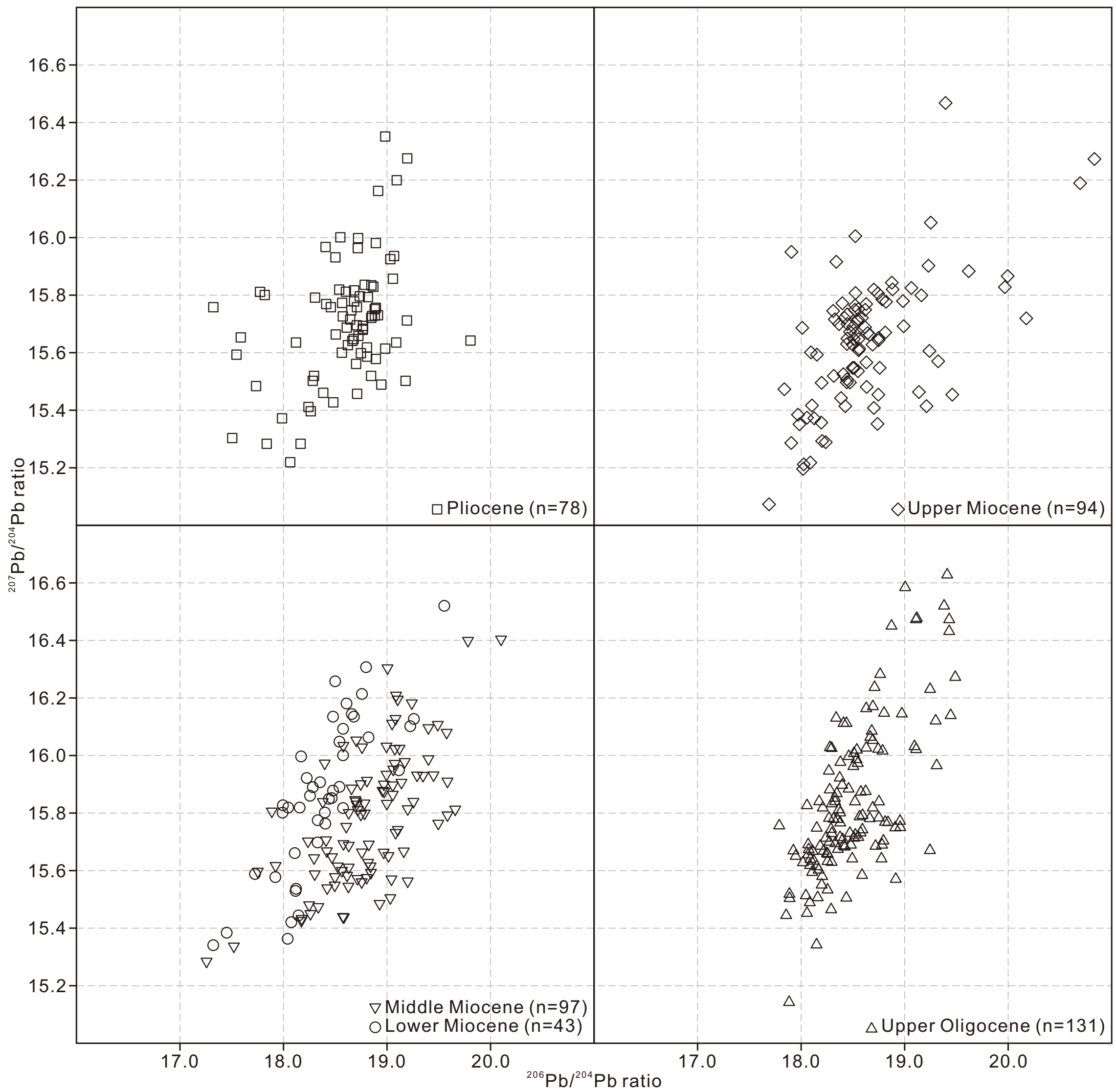
16.6
16.4
16.2
16.0
15.8
15.6
15.4
15.2
Pliocene (n=78)
Upper Miocene (n=94)
Middle Miocene (n=97)
Lower Miocene (n=43)
Upper Oligocene (n=131)
17.0
18.0
19.0
20.0
207Pb/204Pb ratio
206Pb/204Pb ratio

Figure S4

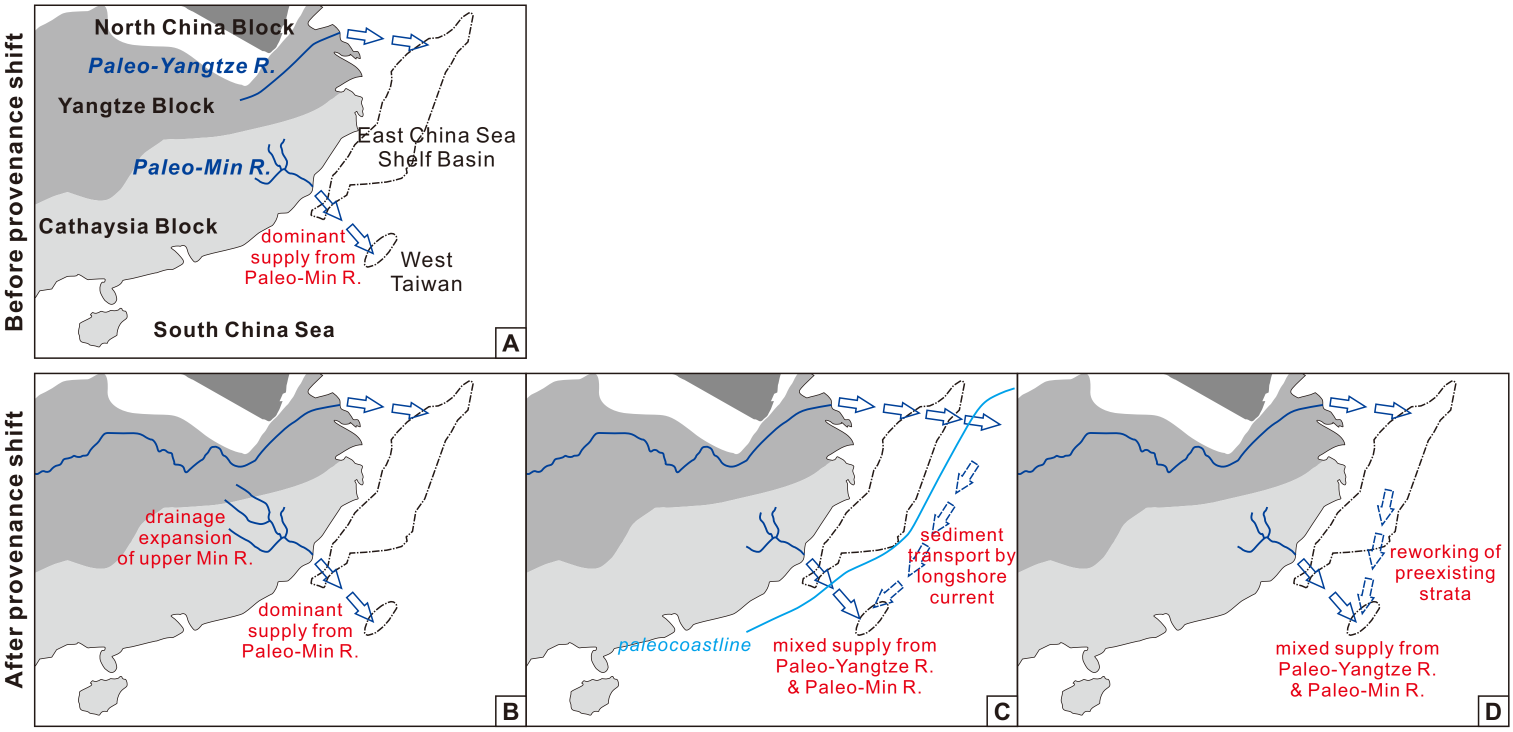
Before provenance shift
North China Block
Paleo-Yangtze R.
Yangtze Block
East China Sea
Shelf Basin
Paleo-Min R.
Cathaysia Block
dominant
supply from
Paleo-Min R.
West
Taiwan
South China Sea
A
After provenance shift
drainage
expansion
of upper Min R.
dominant
supply from
Paleo-Min R.
B
sediment
transport by
longshore
current
paleocoastline
mixed supply from
Paleo-Yangtze R.
& Paleo-Min R.
C
reworking of
preexisting
strata
mixed supply from
Paleo-Yangtze R.
& Paleo-Min R.
D

Figure S5

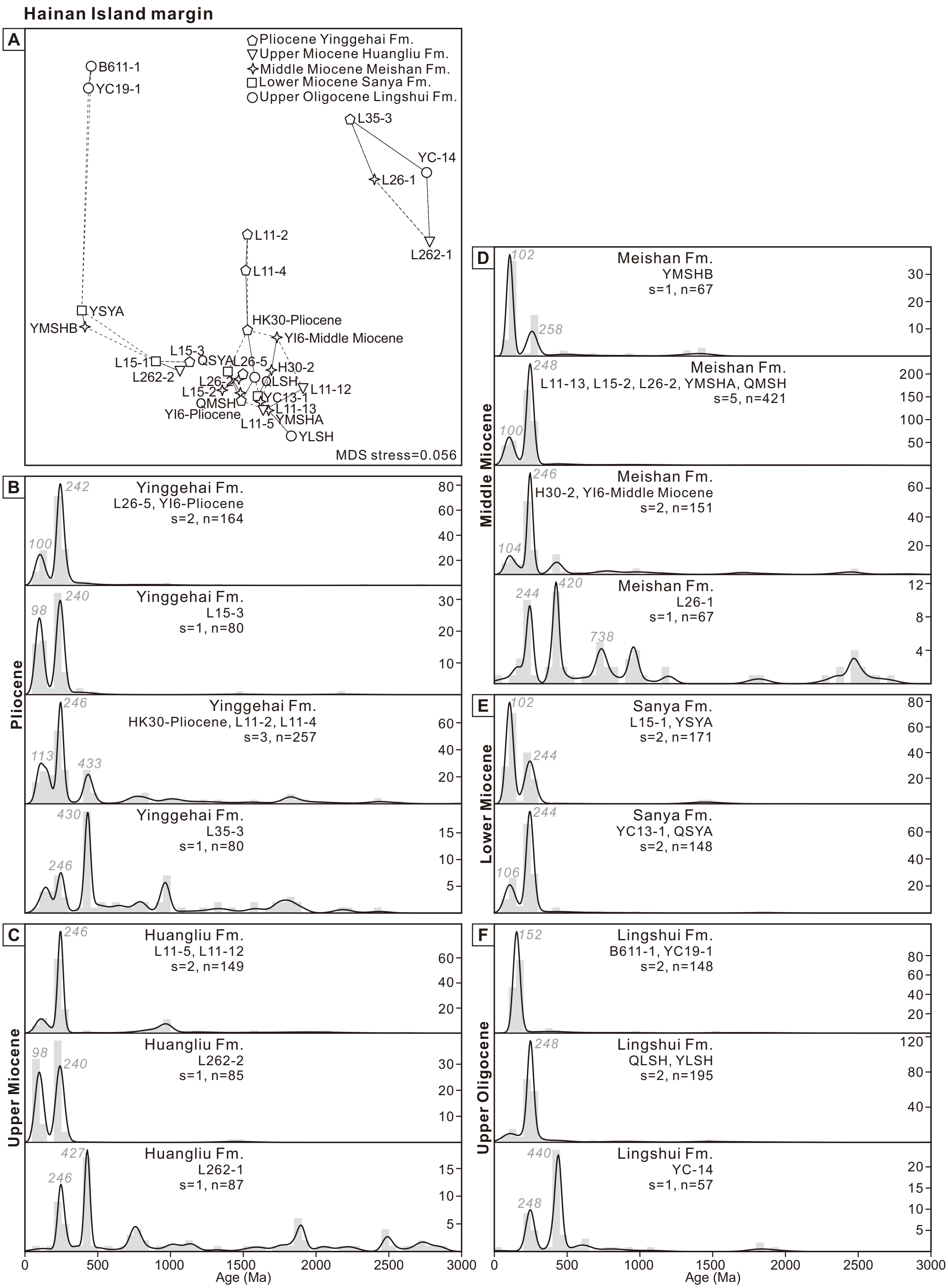
Hainan Island margin
A
Pliocene Yinggehai Fm.
Upper Miocene Huangliu Fm.
Middle Miocene Meishan Fm.
Lower Miocene Sanya Fm.
Upper Oligocene Lingshui Fm.
B611-1
YC19-1
L35-3
YC-14
L26-1
L262-1
L11-2
L11-4
YSYA
YMSHB
HK30-Pliocene
YI6-Middle Miocene
L15-3
L15-1
QSYA
L26-5
L262-2
H30-2
L26-2
QLSH
L15-2
L11-12
YC13-1
QMSH
L11-13
YI6-Pliocene
YMSHA
L11-5
YLSH
MDS stress=0.056
B
Yinggehai Fm.
L26-5, YI6-Pliocene
s=2, n=164
Yinggehai Fm.
L15-3
s=1, n=80
Yinggehai Fm.
HK30-Pliocene, L11-2, L11-4
s=3, n=257
Yinggehai Fm.
L35-3
s=1, n=80
Pliocene
C
Huangliu Fm.
L11-5, L11-12
s=2, n=149
Huangliu Fm.
L262-2
s=1, n=85
Huangliu Fm.
L262-1
s=1, n=87
Upper Miocene
D
Meishan Fm.
YMSHB
s=1, n=67
Meishan Fm.
L11-13, L15-2, L26-2, YMSHA, QMSH
s=5, n=421
Meishan Fm.
H30-2, YI6-Middle Miocene
s=2, n=151
Meishan Fm.
L26-1
s=1, n=67
Middle Miocene
E
Sanya Fm.
L15-1, YSYA
s=2, n=171
Sanya Fm.
YC13-1, QSYA
s=2, n=148
Lower Miocene
F
Lingshui Fm.
B611-1, YC19-1
s=2, n=148
Lingshui Fm.
QLSH, YLSH
s=2, n=195
Lingshui Fm.
YC-14
s=1, n=57
Upper Oligocene
0 500 1000 1500 2000 2500 3000
Age (Ma)

Figure S6

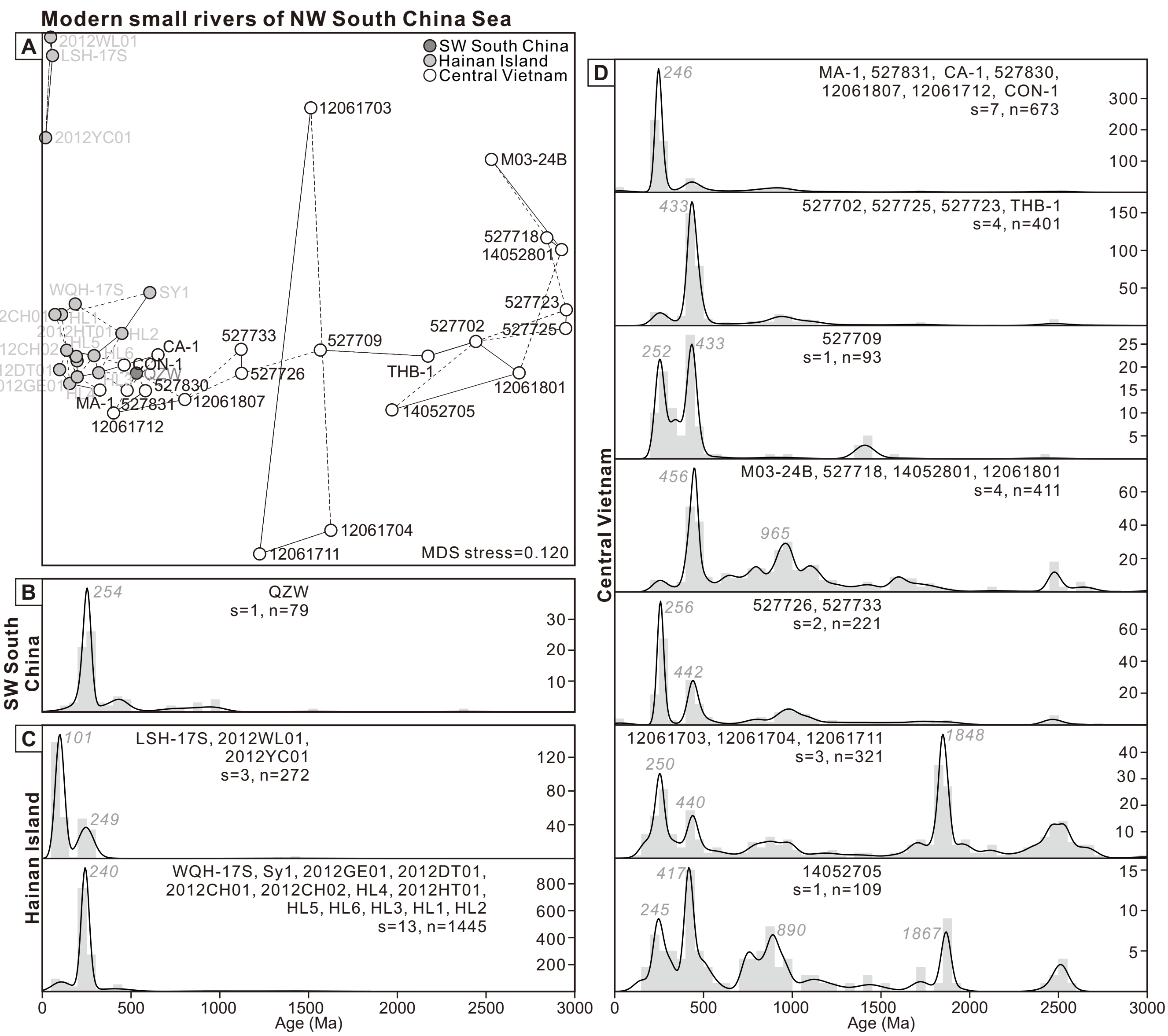

Modern small rivers of NW South China Sea
A
SW South China
Hainan Island
Central Vietnam
MDS stress=0.120
B
SW South China
QZW
s=1, n=79
C
Hainan Island
LSH-17S, 2012WL01, 2012YC01
s=3, n=272
WQH-17S, Sy1, 2012GE01, 2012DT01, 2012CH01, 2012CH02, HL4, 2012HT01, HL5, HL6, HL3, HL1, HL2
s=13, n=1445
D
Central Vietnam
MA-1, 527831, CA-1, 527830, 12061807, 12061712, CON-1
s=7, n=673
527702, 527725, 527723, THB-1
s=4, n=401
527709
s=1, n=93
M03-24B, 527718, 14052801, 12061801
s=4, n=411
527726, 527733
s=2, n=221
12061703, 12061704, 12061711
s=3, n=321
14052705
s=1, n=109
Age (Ma)

Figure S7

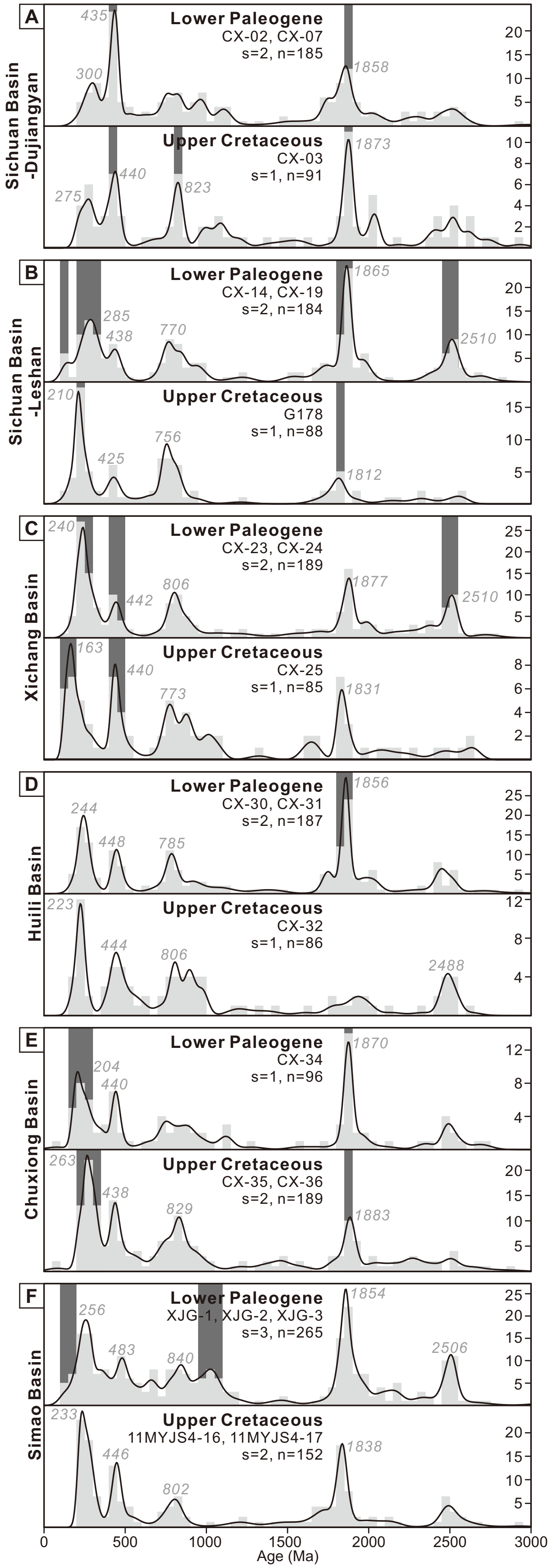

A
Sichuan Basin -Dujiangyan
Lower Paleogene
CX-02, CX-07
s=2, n=185
Upper Cretaceous
CX-03
s=1, n=91
B
Sichuan Basin -Leshan
Lower Paleogene
CX-14, CX-19
s=2, n=184
Upper Cretaceous
G178
s=1, n=88
C
Xichang Basin
Lower Paleogene
CX-23, CX-24
s=2, n=189
Upper Cretaceous
CX-25
s=1, n=85
D
Huili Basin
Lower Paleogene
CX-30, CX-31
s=2, n=187
Upper Cretaceous
CX-32
s=1, n=86
E
Chuxiong Basin
Lower Paleogene
CX-34
s=1, n=96
Upper Cretaceous
CX-35, CX-36
s=2, n=189
F
Simao Basin
Lower Paleogene
XJG-1, XJG-2, XJG-3
s=3, n=265
Upper Cretaceous
11MYJS4-16, 11MYJS4-17
s=2, n=152
Age (Ma)

Figure S8

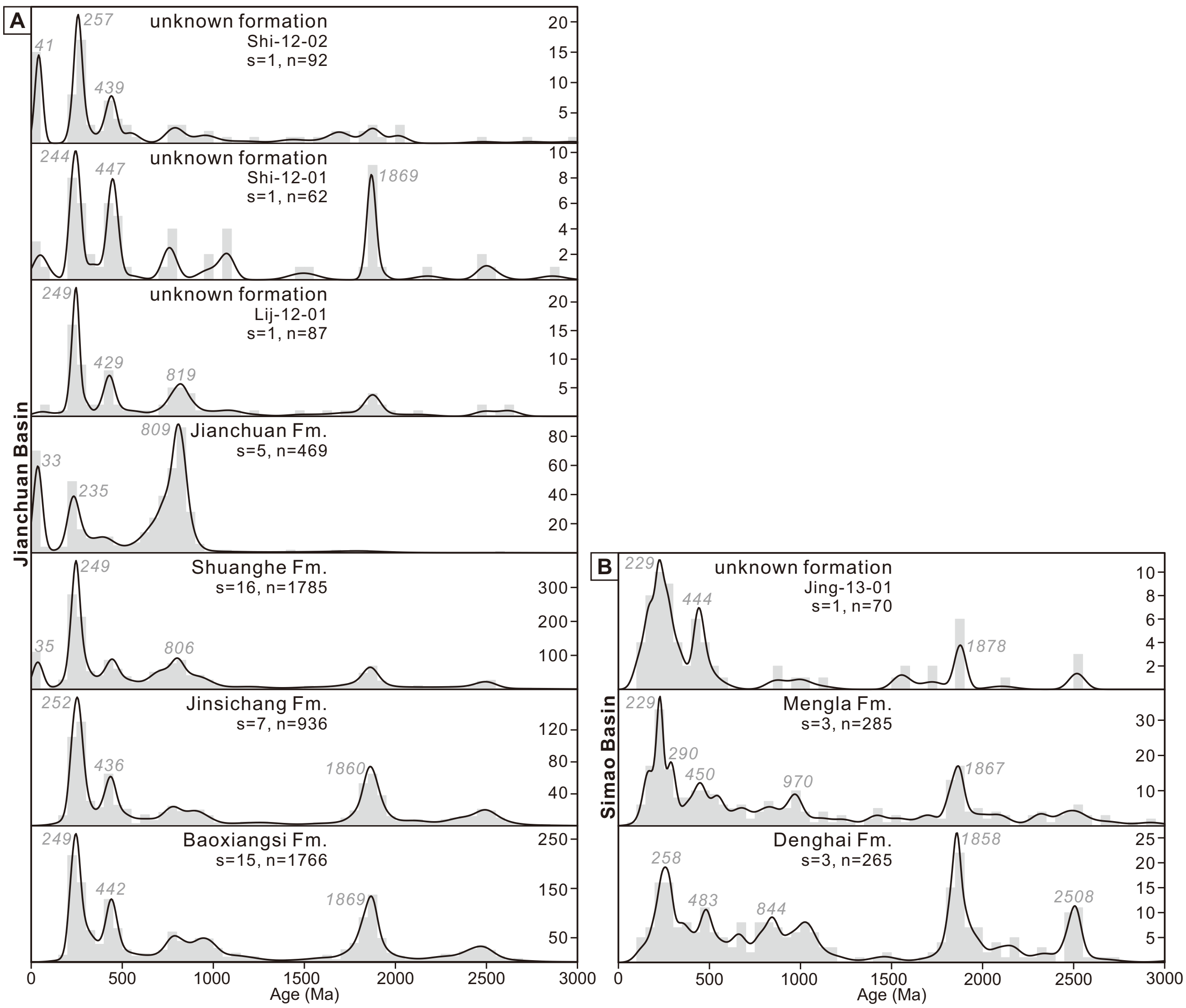

A
Jianchuan Basin
unknown formation
Shi-12-02
s=1, n=92
unknown formation
Shi-12-01
s=1, n=62
unknown formation
Lij-12-01
s=1, n=87
Jianchuan Fm.
s=5, n=469
Shuanghe Fm.
s=16, n=1785
Jinsichang Fm.
s=7, n=936
Baoxiangsi Fm.
s=15, n=1766
Age (Ma)
B
Simao Basin
unknown formation
Jing-13-01
s=1, n=70
Mengla Fm.
s=3, n=285
Denghai Fm.
s=3, n=265
Age (Ma)

Figure S9

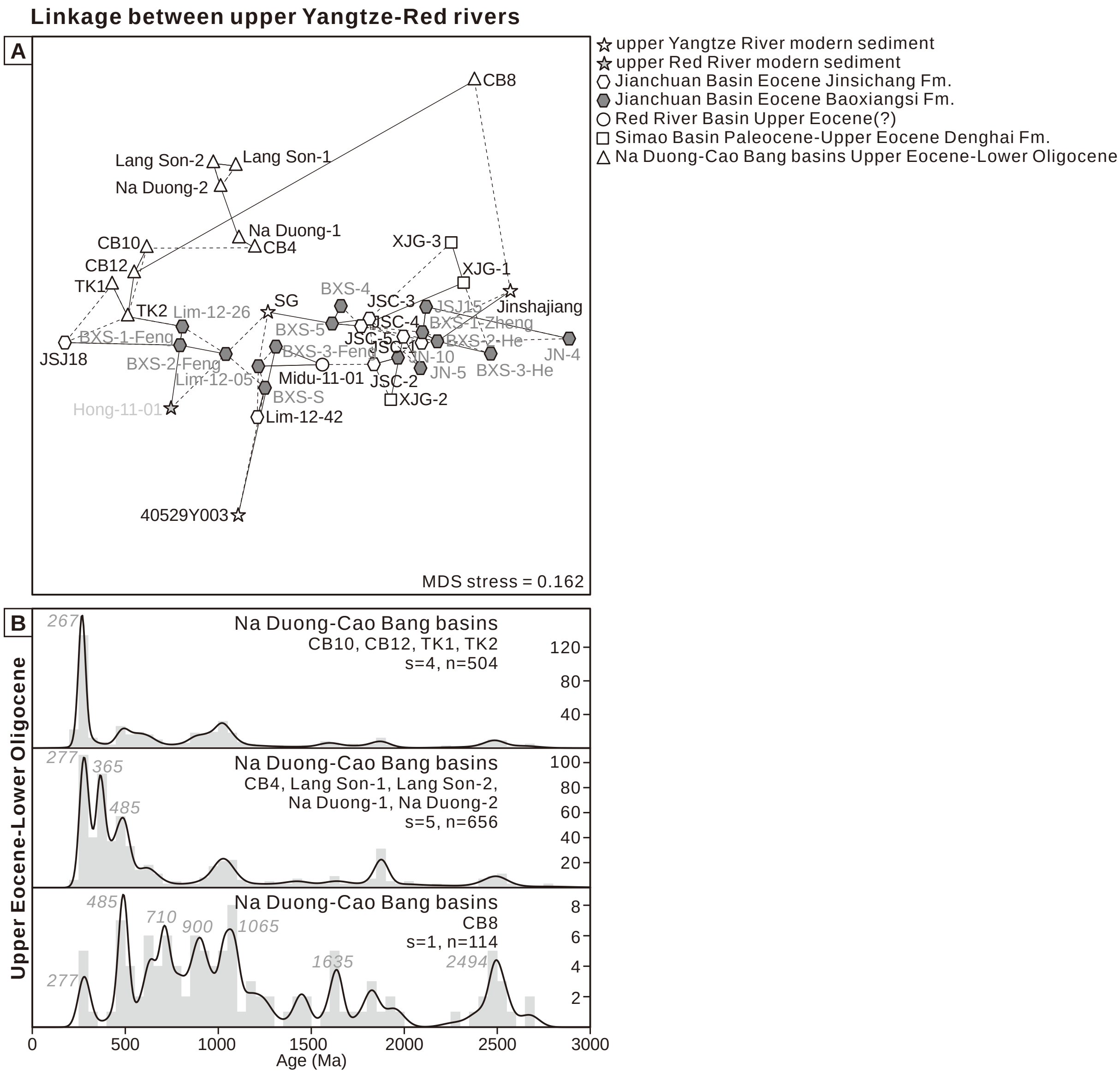

Linkage between upper Yangtze-Red rivers
A
upper Yangtze River modern sediment
upper Red River modern sediment
Jianchuan Basin Eocene Jinsichang Fm.
Jianchuan Basin Eocene Baoxiangsi Fm.
Red River Basin Upper Eocene(?)
Simao Basin Paleocene-Upper Eocene Denghai Fm.
Na Duong-Cao Bang basins Upper Eocene-Lower Oligocene
CB8
Lang Son-2
Lang Son-1
Na Duong-2
Na Duong-1
CB4
CB10
CB12
TK1
TK2
XJG-3
XJG-1
Jinshajiang
SG
Lim-12-26
BXS-4
JSC-3
JSJ15
BXS-1-Zheng
JSC-4
BXS-2-He
JN-4
BXS-1-Feng
JSJ18
BXS-5
BXS-3-Feng
JN-10
BXS-3-He
JN-5
BXS-2-Feng
Lim-12-05
Midu-11-01
JSC-2
XJG-2
BXS-S
Hong-11-01
Lim-12-42
40529Y003
MDS stress = 0.162
B
Upper Eocene-Lower Oligocene
Na Duong-Cao Bang basins
CB10, CB12, TK1, TK2
s=4, n=504
267
Na Duong-Cao Bang basins
CB4, Lang Son-1, Lang Son-2,
Na Duong-1, Na Duong-2
s=5, n=656
277
365
485
Na Duong-Cao Bang basins
CB8
s=1, n=114
277
485
710
900
1065
1635
2494
Age (Ma)

Figure S10

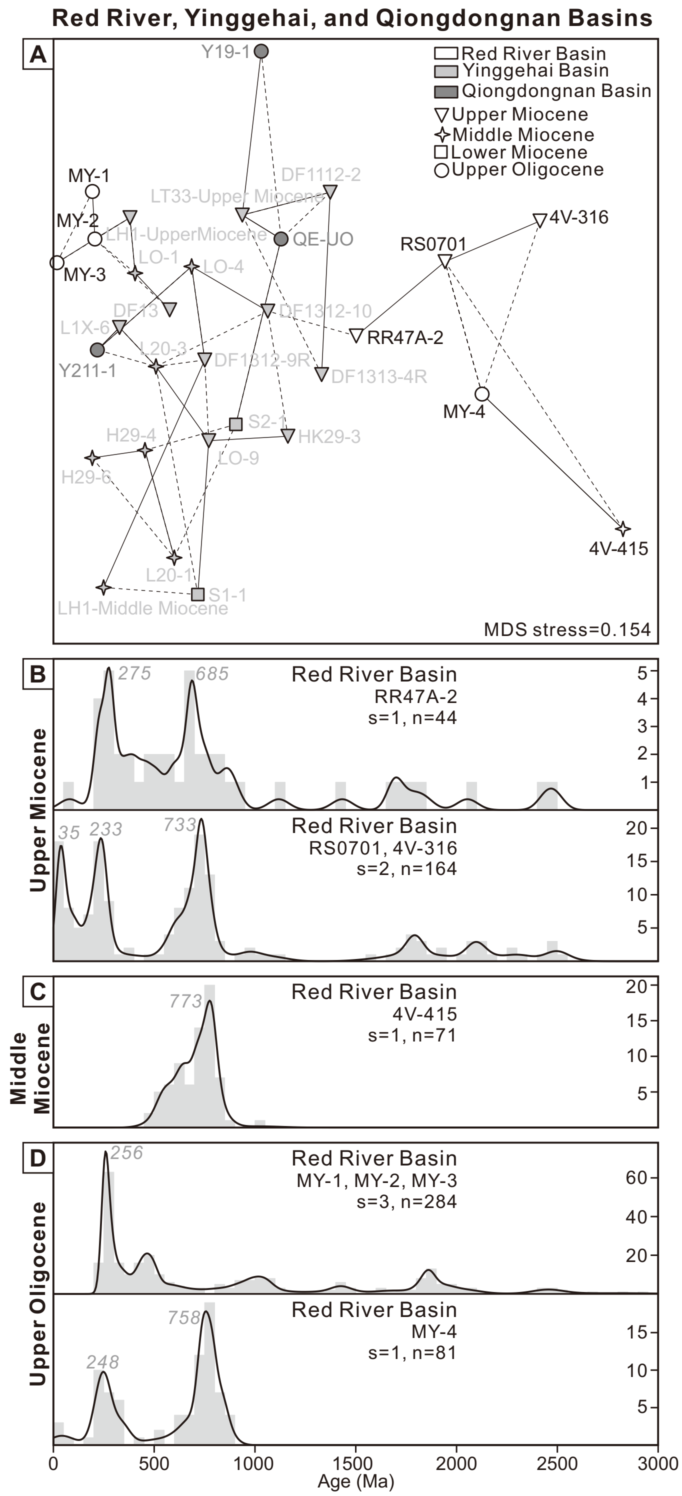

Red River, Yinggehai, and Qiongdongnan Basins
A
Red River Basin
Yinggehai Basin
Qiongdongnan Basin
Upper Miocene
Middle Miocene
Lower Miocene
Upper Oligocene
MDS stress=0.154
B
Red River Basin
RR47A-2
s=1, n=44
Red River Basin
RS0701, 4V-316
s=2, n=164
Upper Miocene
C
Red River Basin
4V-415
s=1, n=71
Middle Miocene
D
Red River Basin
MY-1, MY-2, MY-3
s=3, n=284
Red River Basin
MY-4
s=1, n=81
Upper Oligocene
Age (Ma)

Figure S11

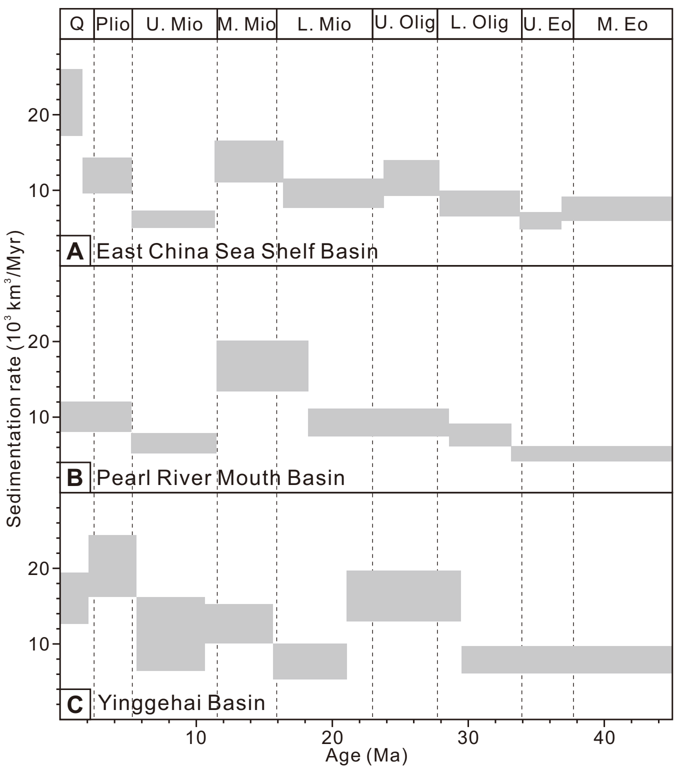

Q
Plio
U. Mio
M. Mio
L. Mio
U. Olig
L. Olig
U. Eo
M. Eo
20
10
A East China Sea Shelf Basin
20
10
B Pearl River Mouth Basin
20
10
C Yinggehai Basin
Sedimentation rate (10³ km³/Myr)
10
20
30
40
Age (Ma)